# When RNA meets montmorillonite: Influence of the pH and divalent cations

Luís de Oliveira, Pollyana Trigueiro, Baptiste Rigaud, Edson da Silva-Filho, Josy Osajima, Maria Fonseca, Jean-François Lambert, Thomas Georgelin, Maguy Jaber

# When RNA meets montmorillonite: influence of the pH and divalent cations

Luís H. de Oliveira[a], Pollyana Trigueiro[b], Baptiste Rigaud[c], Edson C. da Silva-Filho[b], Josy A. Osajima[b], Maria G. Fonseca[a], Jean-François Lambert[d], Thomas Georgelin[e] and Maguy Jaber*[e]

[a]LACOM, Laboratory of Fuels and Materials, UFPB, 58051-085 João Pessoa-PB, Brazil
[b]LIMAV, Interdisciplinary Laboratory of Advanced Materials, UFPI, 64049-550 Teresina- PI, Brazil
[c]CNRS, Institut des Matériaux de Paris Centre (FR2482), 4 place jussieu, 75005 Paris, France
[d]Sorbonne Université, LRS (Laboratoire de Réactivité de Surface), UMR 7197, 4 place Jussieu, F-75005 Paris, France
[e] Sorbonne Université, LAMS (Laboratoire d'Archéologie Moléculaire et Structurale), UMR 8220, Institut Universitaire de France (IUF), 4 place Jussieu, F-75005 Paris, France

*maguy.jaber@upmc.fr

## Abstract

A key question for the investigation of the origins of life is to understand the interaction between complex organic molecules and minerals. In this general frame, the present study investigated the nature of the interactions at the molecular level between a ribonucleic acid and ion-exchanged montmorillonites. We observed that the formation of RNA/clay mineral complexes was strongly pH-dependent. In a sufficiently acidic medium, the RNA molecules were intercalated in the interlayer space, in a flat-lying conformation, with a large contribution of electrostatic interactions that may be complemented by hydrogen bonds. The secondary structure of the RNA strands was strongly affected. The presence of different cations such as $Na^+$, $Ca^{2+}$, $Mg^{2+}$, and $Sr^{2+}$ influenced the adsorption of organic molecules. Apparently, metal cations directly took part in the formation of bridges between the negative charges on the mineral surface and the phosphate groups of the biomolecule.

**Keywords**: Ribonucleic acid, Clay minerals, Montmorillonite, Prebiotic chemistry.

# Introduction

Interactions between biomolecules and clay minerals are key for different fields like separations processes and hybrid nanomaterials. Among clay minerals, montmorillonites belong to the group of smectites with a 2:1 layer structure, negative surface charges (due to isomorphic substitutions), counterbalanced by cations present in the interlayer space, high internal surface area, cation exchange capacity and reactive groups on their surfaces, as well as the ability to confine molecules in the interlayer space (Jaber and Miehé-Brendlé, 2008; Wu et al., 2015; Escamilla-Roa et al., 2017). These intrinsic properties make them possible "hosts" for biomolecules such as RNA (James Cleaves et al., 2012; Ruiz-Mirazo et al., 2014).

The mechanisms of nitrogen bases, nucleotides and RNA/montmorillonite interactions have been reviewed and both electrostatic interactions and hydrogen bonding were found to play a role (Yu et al., 2013). Some studies suggested the participation of the interlayer cations as a “bridge” for interaction between the negatively charged clay surface and the phosphate of the RNA, which also bears a negative charge (Franchi et al., 2003; Pedreira-Segade et al., 2018; Hao et al., 2019). Alkaline earth metal cations have been observed to strongly enhance the adsorption of single-strand (but not double-strand) RNA to montmorillonite (Gujjari et al., 2018). Some studies suggest the likely presence of these metallic cations in rocks and in the primitive ocean (Eder and Rode, 1994; Izawa et al., 2010). They are important for the folding, structure and function of RNA, especially the divalent ion $Mg^{2+}$ (Pyle, 2002; Leonarski et al., 2017), and their involvement has been suggested in the stabilization and/or activation of biological macromolecules (Black et al., 1994). Villafañe-Barajas et al. have also underlined the importance of added cations for the adsorption of nucleotides, the monomers of RNA; and

molecular modelling studies (Carrascoza et al., 2019) suggest that they could play a significant role in the reactivity of adsorbed organic molecules.

pH is a key parameter that controls the adsorption of biomolecules, since acido-basic speciation determines the electrostatic interaction between RNA and the surface (Theng et al., 1982; Lawless et al., 1985). Some studies in recent years have addressed the interaction of nitrogen bases (Benetoli et al., 2008; Hashizume et al., 2010; Carneiro et al., 2011), nucleotides (Feuillie et al., 2013; Pedreira-Segade et al., 2016; Hao et al., 2019) and less often nucleosides (Fornaro et al., 2018) with montmorillonite, varying the pH and the nature of metal cations, and trying to elucidate the types of interactions between these molecules and montmorillonite. However, the interactions of polymeric RNA with the surface of clay minerals remain understudied, especially at the molecular level. In this perspective, the aim of this study was to evaluate the adsorption of RNA (ribonucleic acid diethylaminoethanol salt) on montmorillonite in order to contribute to the understanding of a bigger puzzle, the origin of life. The organic-inorganic interactions were investigated at the molecular level and the influence of different parameters such as nature of the interlayer cation ($Na^+$, $Ca^{2+}$, $Mg^{2+}$, and $Sr^{2+}$) and the pH was evaluated.

# 2. Materials and Methods

## 2.1. Chemicals

Ribonucleic acid diethylaminoethanol salt (diethylethanolammonium; ribonucleic acid derived from Torula yeast, CAS 63231-63-0, Sigma-Aldrich), hydrofluoric acid (HF, 40% w/w, Fluka), sodium acetate ($CH_3COONa$, 99%, Sigma-Aldrich), magnesium acetate ($(CH_3COO)_2Mg.\ 4H_2O$, 99%, Sigma-Aldrich), $Al_2O_3$ (98%, Pural-Sasol), and $SiO_2$ (99.8%,

Aerosil 130, Evonik Industries). The others chemicals were purchased from Sigma-Aldrich (analytical grade). All chemicals were used without any previous purification.

### 2.2. Synthesis of montmorillonite

The sodium montmorillonite (Na-Mt) used in this work was synthesized according to the procedure described previously (Jaber and Miehé-Brendlé, 2005; Jaber and Miehé-Brendlé, 2008; Trigueiro et al., 2018b, 2018a) and had the ideal formula per half unit cell $Na_{0.2}[Si_4Al_{1.8}Mg_{0.2}O_{10}(OH,F)_2]$. The reagents were mixed in the following order: 196.860 g of deionized water, 2.410 g of hydrofluoric acid, 0.990 g of sodium acetate, 2.587 g of magnesium acetate, 3.325 g of alumina and 7.249 g of silica. The obtained hydrogel was aged under stirring at room temperature for 2 h and then was autoclaved at 220°C for 72 h. The autoclave was cooled to room temperature and the product was thoroughly washed with distilled water and centrifuged. Finally, the synthesized Na-Mt was dried at 50°C for 72 h. The synthesis conditions had previously been optimized for the crystallization of pure montmorillonite. The Al/Mg ratio influenced the preferential location of $Al^{3+}$ in the tetrahedral sheets. The initial pH of the hydrogel, around 5, determined the di- or tri-octahedral character of the obtained phyllosilicate and the Si/F ratio as well as the synthesis time influenced the crystallinity of pure montmorillonite (Reinholdt et al., 2001, 2005).

### 2.3. Ion exchange reaction

The ion exchange of Na-Mt was performed according to previously published procedures (Lepoitevin et al., 2014). Na-Mt was suspended in 1 mol $L^{-1}$ of $CaCl_2.2H_2O$, $MgCl_2.6H_2O$ or $Sr(NO_3)_2$ solutions for 24 h under magnetic stirring at 25°C. Then, the obtained materials were centrifuged, washed in deionized water and dried at 50°C. The same process was repeated twice. Finally, the solids were washed and dried in the same conditions. The exchanged montmorillonites will be designated as Ca-Mt, Mg-Mt, and Sr-Mt.

## 2.4. Adsorption of RNA salt on montmorillonite

The adsorption of RNA on the exchanged montmorillonites was performed according to a procedure published previously (Greaves and Wilson, 1969) with some modifications. Initially, the clay mineral samples (Na-Mt, Ca-Mt, Mg-Mt and Sr-Mt) were dispersed in water at a 1.25 mg $mL^{-1}$ concentration over a period of 4 h under magnetic stirring at 25°C. In all cases, the natural pH of all clay mineral dispersions was around 5.0. Then, 1 mg $mL^{-1}$ of RNA solution (pH 6.8) was slowly added. The RNA/Mt ratio was 2:1 w/w for all systems. After this step, the pH of all systems was between 6.2-6.5 without pH adjustment. The system was kept under magnetic stirring for 16 h at 25°C. The same procedure was also performed for all systems at pH 2.9-3.1, adjusted with 0.5 mol $L^{-1}$ of the HCl solution. The resulting samples were centrifuged, washed with deionized water and dried at 50°C overnight. As a control, Na-Mt was maintained at pH 3.0 without RNA in the same conditions and analyzed after the reaction.

## 2.5. Characterizations

**X-ray diffraction (XRD):** powder X-ray diffraction was carried out on a Shimadzu XRD-6000 model diffractometer equipped with a monochromatic CuKα (λ = 0.15406 nm) source operating at 2 kVA, 40 kV, and 30 mA. The diffraction patterns were recorded from 3 to 80° with a scan rate of 0.5° $min^{-1}$ in the same conditions as for previous works (França et al., 2020; da Silva et al., 2021).

**Scanning electron microscopy (SEM):** Scanning electron microscopy was performed using a FEI/Thermo Fischer, model Quanta FEG 250 with cannon per field and an acceleration voltage of 1 to 30 kV. Samples were fixed on carbon tape and coated with gold in a Quorum model Q150R sputter-coater for 35 s at 20 mA by a plasma generated under an argon atmosphere.

**Fourier transform infrared spectroscopy:** the FTIR spectra of samples - dispersed in KBr pellets containing approximately 1% (w/w) of the sample - were recorded using a Shimadzu PESTIGE – 21 model spectrometer over the 4000 – 400 $cm^{-1}$ range at a resolution of 4 $cm^{-1}$ and with 30 scans for each run.

**Thermal analyses (TG-DTG):** Thermogravimetric analyses and derivate thermogravimetry were performed using equipment from TA Instruments SDT Q600 model. The samples were heated from 20 to 1000°C in an alumina crucible with a heating rate of 10°C $min^{-1}$ under nitrogen flow.

**Solid state nuclear magnetic resonance:** $^{31}P$, $^{13}C$, and $^{27}Al$ MAS NMR spectra were obtained on a Bruker Avance III spectrometer equipped with a 4 mm H-X probe, operating at Larmor frequencies of 500.17 MHz ($^{1}H$), 202.47 MHz ($^{31}P$), 125.77 MHz ($^{13}C$) and 130.33 MHz ($^{27}Al$) based on previous studies (Guillermin et al., 2019; Rodrigues et al., 2019; Cavalcanti et al., 2021). Chemical shifts were calibrated using triphenylphosphine (19.64 ppm) for $^{31}P$, the carboxyl signal of adamantane (38.52 ppm) for $^{13}C$, and $AlNO_3$ (0 ppm) for $^{27}Al$ as external standards. All spectra were recorded with a spinning rate of 14 kHz. The $^{13}C$ Cross-Polarization spectra were acquired with a ramp-CP contact time of 2 ms and a 1.5 s recycle delay and with a $^{1}H$ decoupling spinal 64. The acquisition time was 40 ms. The number of scans to obtain the spectra varied depending on the S/N obtained for each sample. Spectra were processed with a zero-filling factor of 2 and with an exponential decay corresponding to a 50 Hz line broadening in the transformed spectra. Only spectra with the same line broadening are directly compared. $^{27}Al$ single-pulse spectra using a 30° pulse were recorded with 100 kHz spectral width and with a recycle delay of 500. $^{31}P$ experiments using a 90° pulse were acquired with a recycle delay of 5 s and with a $^{1}H$ decoupling spinal 64.

# 3. Results

## 3.1. XRD diffraction

XRD patterns of the sodium and exchanged montmorillonites and resulting RNA-Mt hybrids are presented in Figure 1. A reflection at 6.77° (2θ), corresponding to a $d_{001}$-value of 1.30 nm, was observed for Na-Mt. Other reflections were observed at 2θ = 19.91°, 35.31°, 54.71° and 62.13° and were indexed to (110) (0.445 nm), (200) (0.253 nm), (210) (0.167 nm) and (060) (0.149 nm) reticular planes, respectively (Jaber et al., 2014; Trigueiro et al., 2018a). The formation of the Na-Mt was monitored by SEM (Figure SM-1). Well-formed particles in typical plates morphology were observed without the presence of other phases.

For all ion-exchanged samples, the (001) reflections shifted up to 1.56 nm.

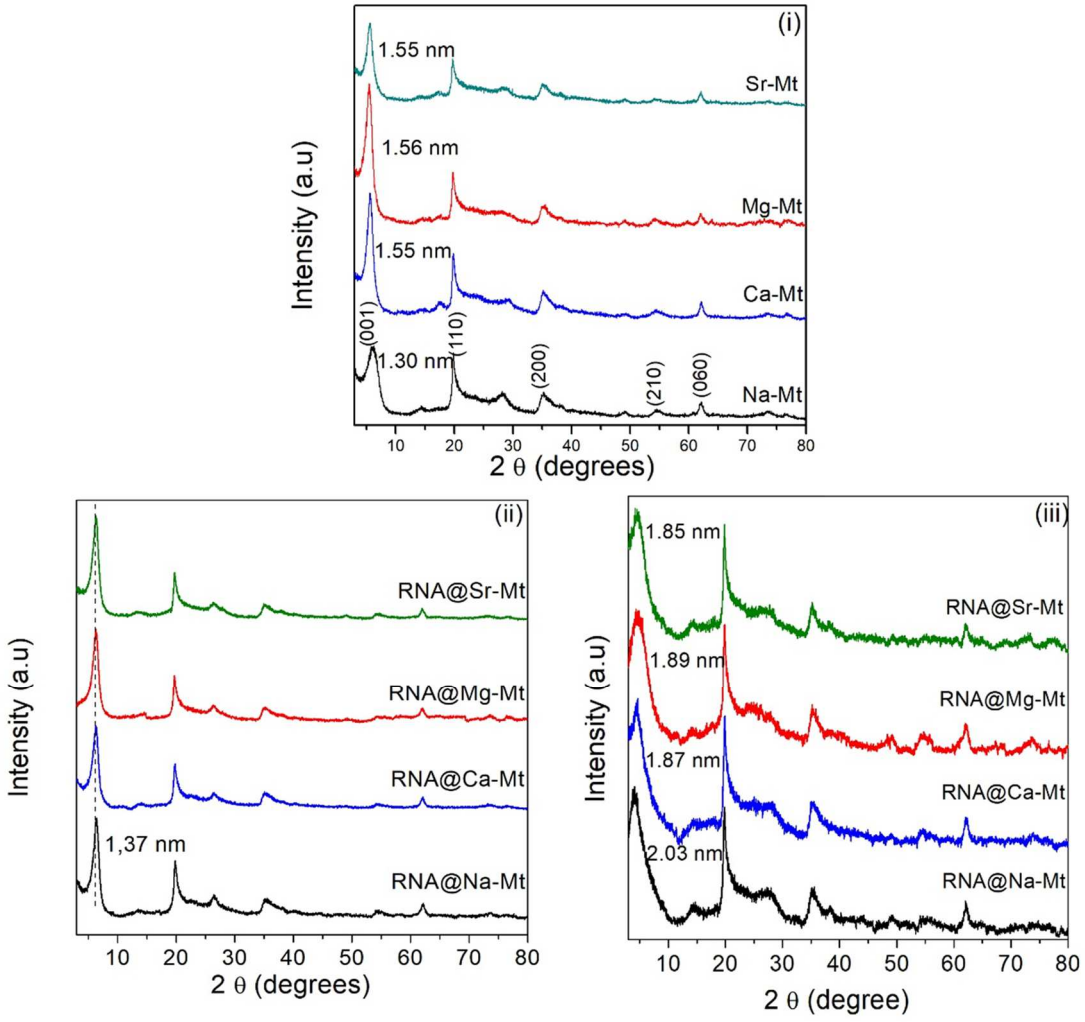


161

162 **Figure 1**:XRD patterns of (i) Na-Mt, Ca-Mt, Mg-Mt, and Sr-Mt montmorillonites and of the
163 RNA@cations-Mt hybrids prepared at (ii) pH 6.2-6.5 and (iii) pH 2.9-3.1.

164

165 After adsorption, the observed pH of the solutions varied between 6.2-6.5 and 2.9-3.1,
166 for systems without and with pH adjustment. Figure 1(ii) depicts the XRD patterns of
167 RNA@cations-Mt at pH 6.2-6.5 and 1(iii) pH 2.9-3.1. At pH 6.2-6.5, the $d_{001}$-value is 1.37
168 nm for all samples. At pH 2.9-3.1, in Figure 1(iii), the (001) reflection shifted to higher basal
169 distances: $d_{001}$-value= 2.03 nm, 1.87 nm, 1.89 nm, and 1.85 nm in RNA@Na-Mt, RNA@Ca-
170 Mt, RNA@Mg-Mt and RNA@Sr-Mt, respectively, corresponding to interlayer spacings in
171 the 0.9 nm range. In contrast, XRD (Figure SM-2) of the Na-Mt maintained in an acidic

medium (pH 3) without the presence of RNA molecules presented the same reflections as the original sample. In particular, the $d_{001}$ value stayed at 1.30 nm and did not show any broadening, suggesting that no alteration in long-range order or formation of exfoliated phase occurred in the conditions of the synthesis.

### 3.2. Infrared spectroscopy

FTIR spectra of the solids before and after RNA adsorption are presented in Figure 2. Irrespective of the compensating cation, the spectra were similar with absorptions at 3638 $cm^{-1}$ and 3400 $cm^{-1}$ (broad) assigned to OH stretching of structural OH and water, respectively (Bizovská et al., 2018). Bands at 1640 and 922 $cm^{-1}$ were attributed to water deformation, and to the OH bending bands in $Al_2OH$, respectively (Madejová et al., 2017).

Absorptions at 1120 $cm^{-1}$ and 1046 $cm^{-1}$ were assigned to Si-O-Si asymmetric and symmetric stretchings, respectively, in the silicate matrix (Bizovská et al., 2018). Two bands at 790 $cm^{-1}$ and 622 $cm^{-1}$ were associated with Al-O-Si bending and to Al-O out-of-plane and Si-O vibrations (Madejová et al., 2017). Furthermore, Al-O-Si and Si-O-Si bending modes were observed at 528 and 471 $cm^{-1}$, respectively (Pentrák et al., 2018). If amorphous silica was present, it would be detected by absorption bands at 800 - 810 $cm^{-1}$ (Costa et al., 1997; Pentrák et al., 2012; Santos et al., 2015); they were not observed in present case.

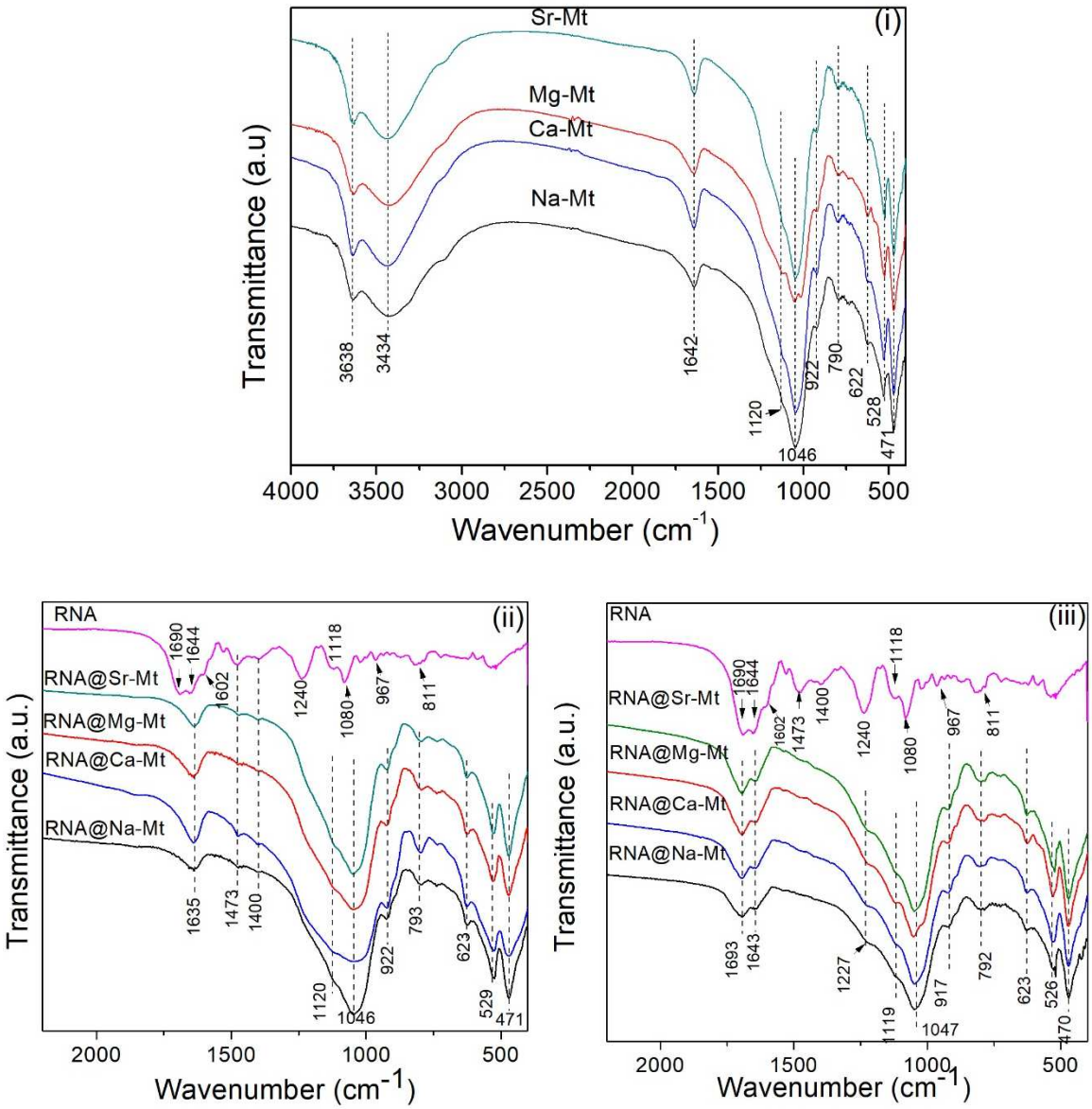


**Figure 2**. FTIR spectra for (i) Na-Mt, Ca-Mt, Mg-Mt and Sr-Mt montmorillonites, and spectra in range 2200 – 400 $cm^{-1}$ for RNA and RNA@cations-Mt hybrids obtained at (ii) pH 6.2-6.5 and (iii) pH 2.9-3.1.

Figure 2ii and iii shows FTIR spectra in the 400-2000 $cm^{-1}$ range of RNA and solids after RNA adsorption. FTIR spectra in the complete 400-4000 $cm^{-1}$ range are presented in Figures SM-2i and ii. The spectrum of RNA presents a band at 3387 $cm^{-1}$ (Figure SM-2i and ii) associated with the N-H stretch and one at 2954 $cm^{-1}$ due to the C-H stretch (Tsuboi, 1970). The bands at 1690, 1644 and 1602 $cm^{-1}$ were associated with the C=O vibration on

200 purine and pyrimidines (Tsuboi, 1970; Banyay et al., 2003). The absorption band at 1473 $cm^{-1}$
201 has been attributed to ring vibrations of the uracil base (Kumar and Singh, 2013) and the one
202 at 1400 $cm^{-1}$ was attributed to in-plane C-O-H deformation mode, at 2' in the ribose ring
203 (Tsuboi, 1970; Banyay et al., 2003). The bands at 1240 and 1080 $cm^{-1}$ were attributed to
204 asymmetrical and symmetrical $PO_2^-$ stretch, respectively (Tsuboi, 1970; Benedetti et al., 1997)
205 and the band at 1118 $cm^{-1}$ to the C-O stretch in ribose (Benedetti et al., 1997). Finally, the
206 band at 967 $cm^{-1}$ is an unidentified ribose-phosphate main chain vibrations, and that at 811
207 $cm^{-1}$ is a sugar marker of complex origin (Tsuboi, 1970; Banyay et al., 2003).

208 The spectra of the solids after RNA adsorption in the 400-2000 $cm^{-1}$ range are
209 depicted in Figures 2ii and iii. At pH 6.2-6.5 (Figure 2ii), similar new bands were observed in
210 the FTIR spectra of the solids, both at the same position as in the spectra of RNA: 1473 $cm^{-1}$
211 (ring vibrations) and 1400 $cm^{-1}$ (in-plane C-O-H deformation of ribose). Other diagnostic
212 bands of RNA may be present as shoulders, but are hidden by the strong absorption of the
213 clay mineral lattice in the 900-1200 $cm^{-1}$ region.

214 Infrared spectra of the hybrids obtained in an acidic medium (Figure 2iii) showed
215 different additional bands at 1693 $cm^{-1}$ (C=O stretching in nucleobases). The band of $PO_2^-$,
216 observed at 1240 $cm^{-1}$ in RNA spectra (Figure 3), shifted to 1227 $cm^{-1}$ in the RNA@cations-
217 Mt.

218 Bathochromic shifts of the bands attributed to the structural OH of the clay mineral
219 lattice (cations-Mt: 3638 $cm^{-1}$, RNA@cations-Mt at pH 6.2-6.5: 3632 $cm^{-1}$ and
220 RNA@cations-Mt at pH 2.9-3.1: 3630 $cm^{-1}$), were observed (see Supplementary materials
221 Fig. SM-3i and ii).

### 3.3. $^{27}$Al, $^{13}$C and $^{31}$P solid state NMR

$^{27}$Al NMR spectra for samples before and after adsorption of the biomolecule at pH 2.9-3.1 are shown in Figure 3i and ii. All precursor samples presented characteristic chemical shifts at 3.9 and 69.1 ppm. Another chemical shift was observed in both spectra at 55 ppm. The same chemical shifts were observed in the RNA@cations-Mt samples.

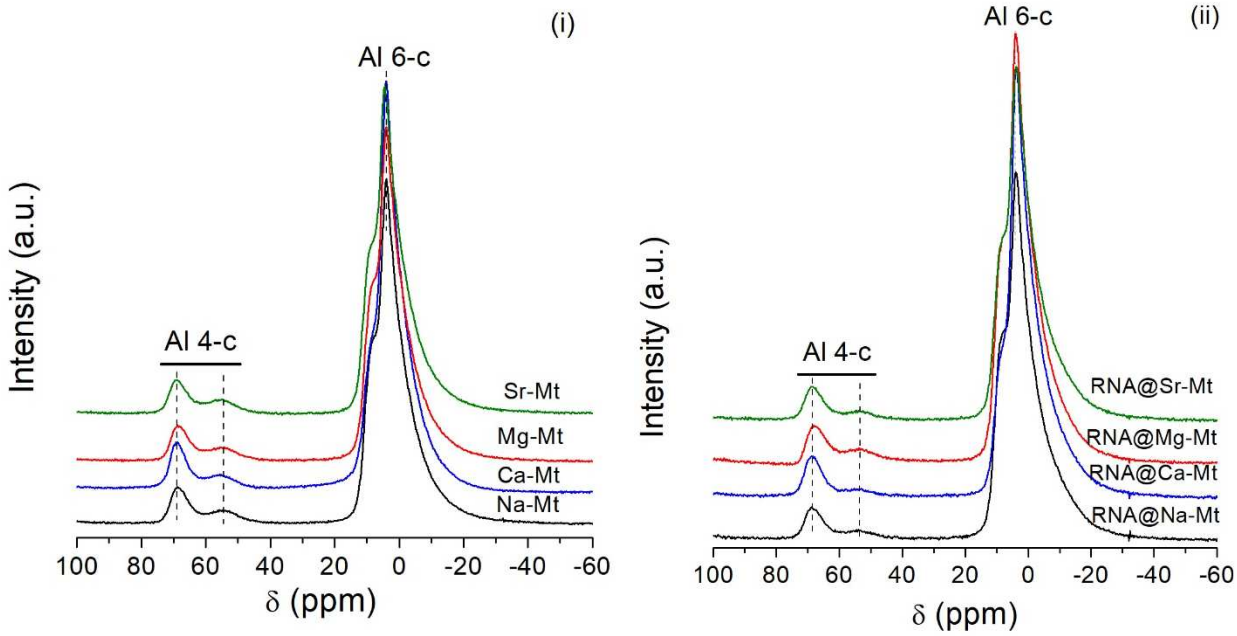


**Figure 3**. $^{27}$Al NMR spectra of the (i) exchanged montmorillonites and (ii) RNA@Mt hybrids obtained at pH 2.9-3.1.

The $^{31}$P spectrum of RNA is shown in Figure 4i. A broad, asymmetric signal is observed with a maximum at +1.4 ppm. For the RNA@cations-Mt samples, a strong new component appeared at -9.3 to -10.6 ppm, i.e., 8 to 9 ppm upfield from the signal in pristine RNA.

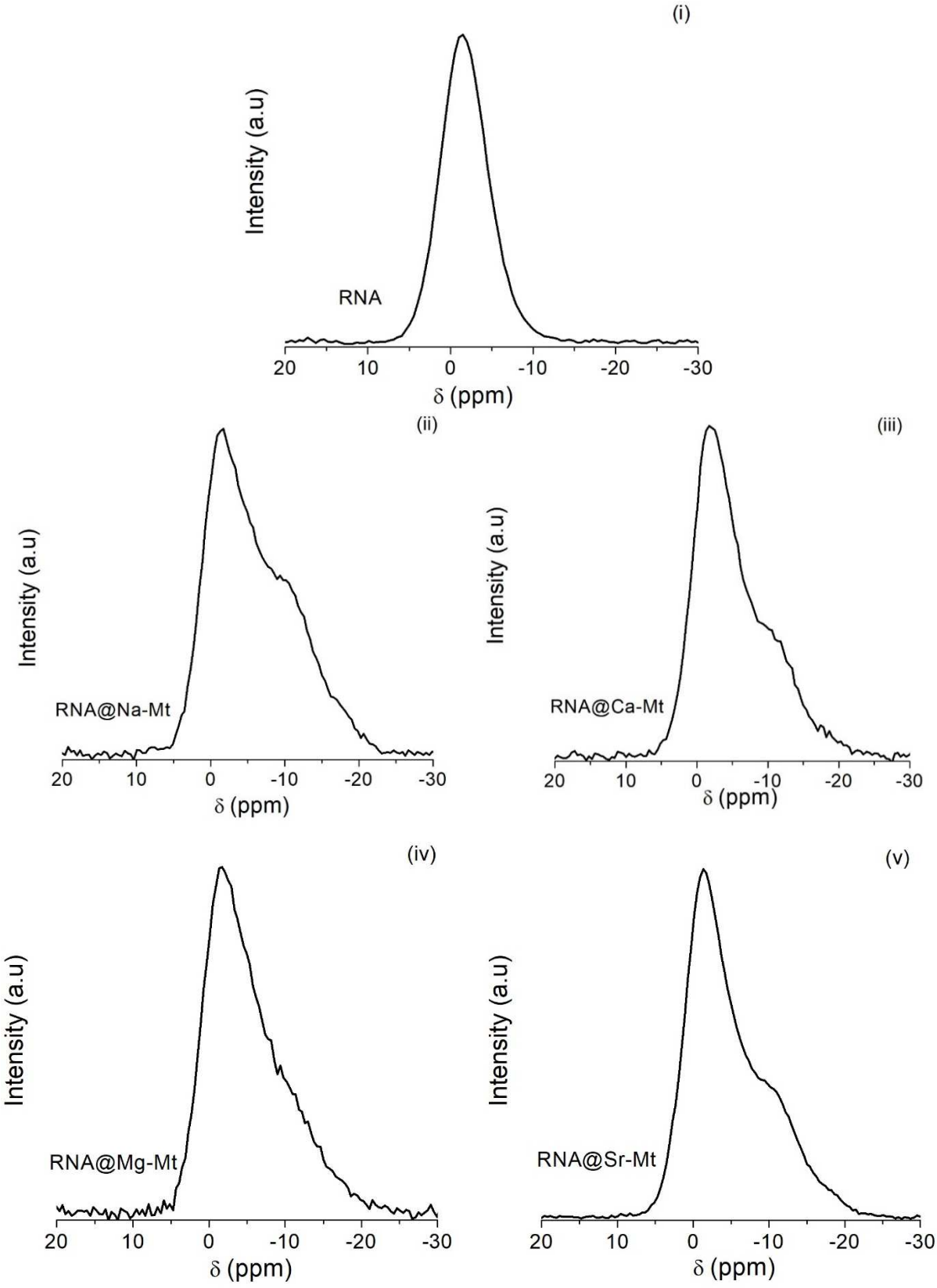


237 **Figure 4**. $^{31}$P NMR spectra of RNA (i) and hybrids RNA@Na-Mt (ii), RNA@Ca-Mt (iii),
238 RNA@Mg-Mt (iv) and RNA@Sr-Mt (v) in pH 2.9-3.1.

239

240 $^{13}C$ NMR spectra of the RNA and the hybrids obtained at pH 2.9-3.1 are depicted in
241 Figure 5 and values of chemical shifts and respective attributions are summarized in Table 1.
242 The observed NMR signals for the RNA@Mt hybrids were similar.

243 The signals at 60 – 90 ppm were assigned to carbons in the ribose moiety (Chang et
244 al., 1982; Rodrigues et al., 2019). Signals in the 100 - 170 ppm range were attributed to the
245 nucleotides bases (Chang et al., 1982; Fujiwara et al., 1995). In particular, the signals of
246 carbon positions $G_4$ and $A_4$ were located at 150.3 ppm, and were assigned to C=C groups in
247 both nucleotides bases. This signal was also present in the RNA@Mt hybrids, but shifted to
248 151.5 ppm. The signal at 165.4 ppm associated with the carbon at position 4 in cytosine (-
249 ($NH_2$) C=N) group, shifted to 166.4, 166.6, 166.4, and 166.5 ppm, in the RNA@Na-Mt,
250 RNA@Ca-Mt, RNA@Mg-Mt, and RNA@Sr-Mt, respectively. The other well-individualized
251 signals did not shift as much.

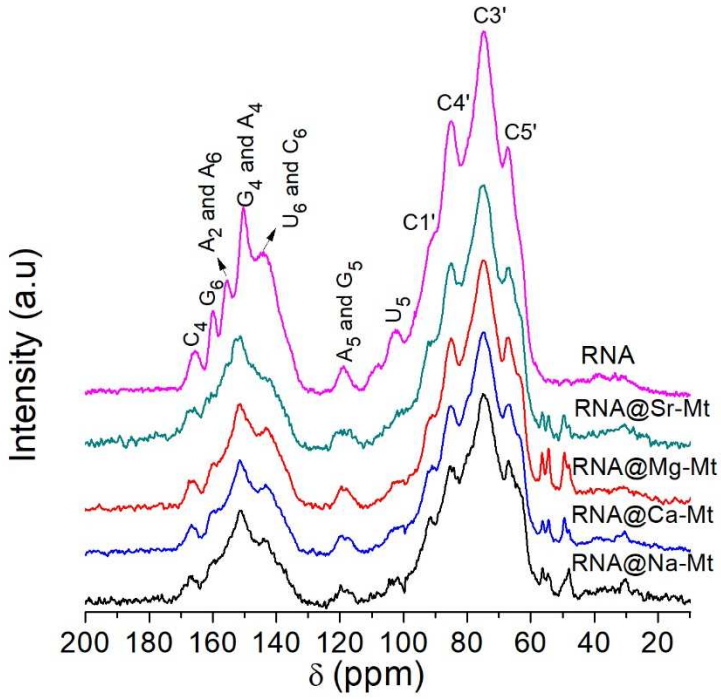


252

**Figure 5**. $^{13}C$ NMR spectra of the RNA and RNA@Mt hybrids obtained at pH 2.9-3.1 (The symbol C' represents the carbons present in the ribose group and $U_5$, for example, represents the carbon 5 in the uracil nitrogen base).

**Table 1**. $^{13}C$ chemical shifts of RNA and RNA@clay hybrids in pH 2.9-3.1*.

| RNA | RNA@Na-Mt | RNA@Ca-Mt | RNA@Mg-Mt | RNA@Sr-Mt | Attributions |
|---|---|---|---|---|---|
| 67.2 | 67.0 | 67.1 | 67.1 | 67.1 | C5'[a] |
| 74.7 | 74.7 | 74.8 | 74.8 | 74.9 | C3'[b] |
| 85.0 | 85.0 | 85.0 | 85.0 | 85.0 | C4'[a] |
| 91.2 | 91.4 | 91.2 | 91.4 | 91.5 | C1'[b] |
| 102.5 | 102.7 | 102.6 | 102.6 | 102.4 | U5[b] |
| 119.0 | 119.0 | 119.0 | 119.0 | 119.0 | A5 and G5[b] |
| 144.1 | 143.9 | 144.0 | 143.9 | 143.8 | C6 and U6[b,d] |
| 150.3 | 151.5 | 151.5 | 151.5 | 151,5 | G4 and A4[b] |
| 155.4 | - | - | - | - | A2 and A6[b,c] |
| 159.8 | 159.7 | 159.5 | 159.5 | 160.0 | G6[d] |
| 165.4 | 166.4 | 166.6 | 166.4 | 166.5 | C4[b] |

**Chemical Shifts in ppm.* [a](Rodrigues et al., 2019); [b](Chang et al., 1982); [c](Fujiwara et al., 1995); [d](Lapper et al., 1973). *C' refers the carbons of the ribose group; A4, C4, U4 and G4 for example, refer to carbon 4 in the adenine, cytosine, uracil, and guanine nitrogen base, respectively.*

### 3.4. Thermogravimetry

TG and DTG curves of the solids before and after RNA adsorption at pH 2.9-3.1 are presented in Figure SM-3, and summarized in Table SM1. It was hoped that the amount of intercalated RNA could be estimated by integrating the weight losses after 200°C and correcting for the weight loss of the raw montmorillonite clay. Some thermal events attributable to the degradation of RNA are indeed apparent between 200 and 460°C, but organic matter elimination is not complete even at 1000°C, so that the amounts tabulated are to be interpreted as lower bounds. They appear to be only little sensitive to the nature of the compensation cation, or even to its charge.

# 4. Discussion

### *XRD diffraction*

The XRD patterns of the sodium montmorillonite confirm the expected dioctahedral character of the sample according to the 2θ = 62.13° reflection, indexed (060) plane; in other words, they indicate the predominance of trivalent cations in the octahedral sheet of Na-Mt (Moore and Reynolds, 1997; Reinholdt et al., 2001, 2005). For the exchanged samples, the observation of the (001) reflections at 1.56 nm for all samples are compatible with a two-layer hydrate in the interlayer, as compared to a one-layer hydrate in the starting material (Cases et al., 1997; Cavalcante et al., 2016; Chang et al., 2018).

After RNA adsorption, there is no intercalation of bulky species in the interlayer space in the pH 6.2-6.5 systems, as the $d_{001}$ still corresponds to a two-water layer hydrate. The possibility of intercalation strongly depends on the electrostatic interactions between the clay mineral layers (negatively charged) and the molecule to be intercalated. Individual nucleotides exhibit two or three acid-basic couples due to the protonation/deprotonation of nucleobase nitrogens and of the bridging phosphate P-OH (Martin, 1985; Feuillie et al., 2013). Deprotonation of the heterocycle NH group is possible for GMP and UMP nucleotides (pKa = 9.4 to 9.5) but this equilibrium is not active in our pH conditions. The nucleobases may be protonated in the cases of AMP (N1, p$K_a$ = 3.84), CMP (N3, p$K_a$ = 4.33) and GMP (N7, p$K_a$ = 2.48) (Feuillie et al., 2015). This part of the nucleotides would then be mostly neutral at pH 6.2 to 6.5, while at pH 2.9 to 3.1, the majority of AMP and CMP groups, and a minority of the GMP (20 to 30%) would be protonated. Finally, the phosphate group has a pKa of the order of 0.5 and is always deprotonated in our conditions.

Thus, in a neutral medium, each nucleotide residue would bear a net negative charge of -1 and the intercalation of the biopolymer would be electrostatically disfavored because of

296 repulsive interactions with the negative clay mineral layers, since in all pH conditions,
297 montmorillonite has a negative charge (Saka and Güler, 2006; Yukselen and Erzin, 2008; Liu
298 et al., 2017; Şans et al., 2017; Guillermin et al., 2019). It is therefore likely that RNA
299 molecules at pH 6.2-6.5 are adsorbed on the external surface and edges of the clay mineral
300 samples (Mignon et al., 2009; Mignon and Sodupe, 2012). In addition, the cations ($Na^{+}$, $Ca^{2+}$,
301 $Mg^{2+}$ and $Sr^{2+}$) may be contributing to adsorption, by creating "ion bridges" between the
302 negative surface of montmorillonite and the phosphate groups present in RNA. A similar
303 mechanism was invoked for the adsorption of DNA in montmorillonite in the presence of
304 different cations (Sheng et al., 2019).

305 For the system at pH 2.9-3.1, higher basal reflections were observed for all samples,
306 indicating the intercalation of a rather large biomolecule in the interlayer space of the clay
307 mineral. The occurrence of intercalation is associated with the partial protonation of the
308 nitrogen bases in the RNA nucleotides at pH values lower than their pKa. With the pKa
309 values listed above, and supposing that the four possible nucleotide monomers have similar
310 abundances in the RNA chain, it is easy to calculate that at pH 2.9-3.1, the chain bears a
311 charge that is reduced by over one half with respect to pH 6.2-6.5 – about 0.48 negative
312 charges per monomer. In these conditions, electrostatic repulsion between the RNA chain and
313 the negatively charged surface is reduced, permitting intercalation. These interpretations are
314 compatible with other studies in RNA adsorption (Greaves and Wilson, 1969; Jelavić et al.,
315 2017) and also studies about the adsorption of the nitrogen bases (Carneiro et al., 2011) and
316 nucleotides (Pedreira-Segade et al., 2016) on montmorillonite. Similar results were observed
317 in the RNA intercalation in montmorillonite in an acidic medium (pH 5 to 3.5) (Greaves and
318 Wilson, 1969). Other studies observed no displacement of the basal plane in torula yeast
319 RNA/Mg-smectite (Viennet et al., 2020) and DNA/ion-exchanged Mt ($Li^{+}$, $Na^{+}$, $Mg^{2+}$, $Ca^{2+}$,
320 $Fe^{3+}$ and $Al^{3+}$) Mt (Xie et al., 2019)., but they were not conducted at low pH.

It is obvious that what is intercalated is not the intact torula yeast RNA, which has an intricate ternary structure and exists in solution as a Y-shaped molecule (Tripathi et al., 2017) with a 30 nm gyration radius (Manzano and Zydney, 2017). Indeed, a double strand of nucleic acid has a diameter of about 26 Å, and consequently, even a single strand lying in the interlayer with its nucleobases perpendicular to the clay layers would give an interlayer spacing of about 13 Å, significantly higher than the values we observe. This is why in the structural sketch of intercalated RNA we propose in Figure 6, the RNA strand is represented with the bases lying flat in the interlayer. This would involve a strong degree of RNA deformation; therefore, it is likely that the whole RNA molecule does not enter the interlayer. It is proposed that only fragments of the RNA chain are intercalated, while the rest of the molecule may be adsorbed on the surface or edges of the Mt. A similar adsorption mechanism has been documented for other biomacromolecules in Mt, such as enzymes (Sanjay and Sugunan, 2006; Gopinath and Sugunan, 2007).

***Infrared spectroscopy***

At both pHs, new bands were observed in the FTIR spectra of samples after the absorption of RNA. For example, at pH 6.2-6.5, bands assigned to ring vibrations and in-plane C-O-H deformation of ribose were observed. At pH 2.9-3.1, new bands assigned to C=O and $PO_2^-$ stretching were apparent. Furthermore, changes in the position of the $PO_2^-$ band were observed. This shift is probably associated with distortions in the RNA molecule, possibly caused by the interactions of cations with phosphate groups (Duguid et al., 1993; Andrushchenko and Bouř, 2009; Pedreira-Segade et al., 2018). It is likely that the clay/RNA interaction simultaneously includes several contributions from different local interactions such as H-bonds. It may be relevant from this point of view that the stretching vibration of the clay layer structural O-H shifts by a few $cm^{-1}$, which may be indicative of their implication in

H-bonding (Schnetzer et al., 2017), but a more precise study would be needed to identify H-bonds with confidence.

### *$^{27}$Al, $^{13}$C and $^{31}$P solid state NMR*

$^{27}$Al NMR spectra in all precursor samples presented characteristic chemical shifts at 3.9 and 69.1 ppm related to hexacoordinated (Al 6-c) and tetracoordinated (Al 4-c) aluminum located in octahedral and tetrahedral sheets of the Mt, respectively (Cadars et al., 2012; Marsh et al., 2018). Another chemical shift corresponding to the Al 4-c environment was observed in both spectra at 55 ppm and can be attributed to small impurities of amorphous aluminosilicate, also observed in the literature for synthetic (Cadars et al., 2012) and natural (Garg and Skibsted, 2014) montmorillonites. In the RNA@cations-Mt samples (Figure 3ii), no change was observed with respect to cations-Mt, indicating the absence of interaction between the biomolecule and Al sites in the Mt.

As regards the $^{31}$P spectrum of RNA, Figure 4i, there are surprisingly few literature results available for comparison. Solution studies of short RNA sequences (Legault and Pardi, 1994; Maderia et al., 2000) revealed a series of narrow peaks in the (+2.0, -2.0) ppm range corresponding to all different phosphodiester bridges in the RNA chain. In the solid state, the loss of resolution may produce a signal such as the one we are observing. For the RNA@cations-Mt samples, a strong new component appeared. This finding is quite unexpected since the shift is comparable to the chemical shift difference separating the $Q^0$ signal in monophosphate from the $Q^1$ in diphosphate. The formation of diphosphate seems unlikely however, as it would require a breakdown and rearrangement of the RNA structure. Another possibility is that the new signal could correspond to the effect of the adsorption interaction on the bridging phosphate groups. Among likely interactions, only coordinative bonds to metal cations would be expected to result in such shifts. Intuitively, however, they

370 would also be expected to induce a decrease in electron density in the phosphate moiety, and
371 therefore a downfield shift (increase in chemical shift values) – the opposite of the effect
372 observed here. The already quoted study by Maderia et al (2000) indeed reports shifts of
373 several ppm when modified hairpin RNA is contacted with $Cd^{2+}$ or $Mg^{2+}$ cations. For
374 different RNA structures, they can be either upfield or downfield. The authors could not
375 provide any clear explanation for the upfield shifts; they supposed that the affected phosphate
376 groups did not directly coordinate to the cations, but were indirectly affected through changes
377 in RNA conformations. We will not speculate any further on the reasons for the new signal
378 observed here, except to say that it reveals a strong RNA/clay mineral interaction. One can
379 also note that in at least three of the four samples, there are indications of a third, even more
380 upfield shifted component in the $^{31}P$ spectrum; attempts at signal deconvolution necessitated
381 the introduction of a component at -14 to -17 ppm. The hypothesis of strong deformations of
382 the RNA chain is in line with the structural picture deduced from XRD.

383 The $^{13}C$ NMR spectra show chemical shifts values that are practically the same for
384 the different montmorillonites. This suggests that the nucleotide bases, mainly adenine and
385 cytosine, can be protonated in an acidic medium (pH 2.9-3.1). These results are in keeping
386 with calculations based on the pKa values. They corroborate the FTIR and XRD results,
387 indicating that the protonation of these moieties induces hydrogen bonds and electrostatic
388 interactions with the montmorillonite surface.

389 Figure 6 sketches a model of the RNA-clay composites that is compatible with the
390 information from XRD, IR and $^{13}C$ and $^{31}P$ NMR.

391

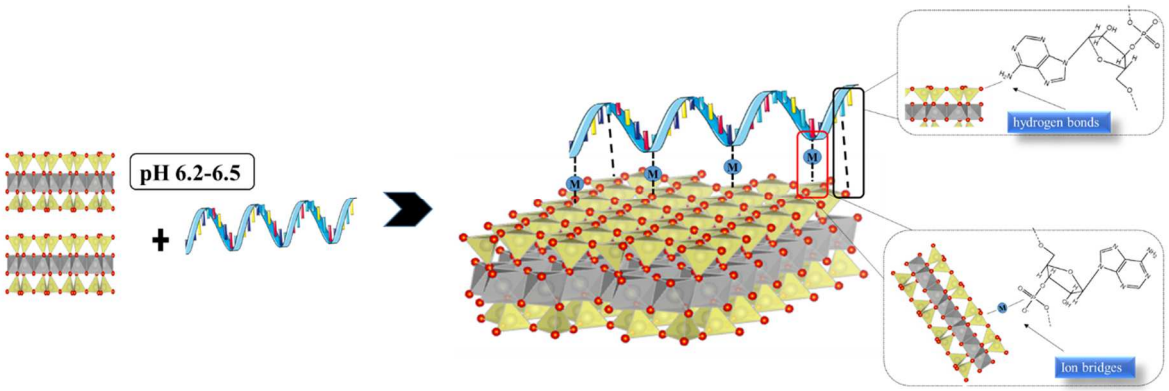


392

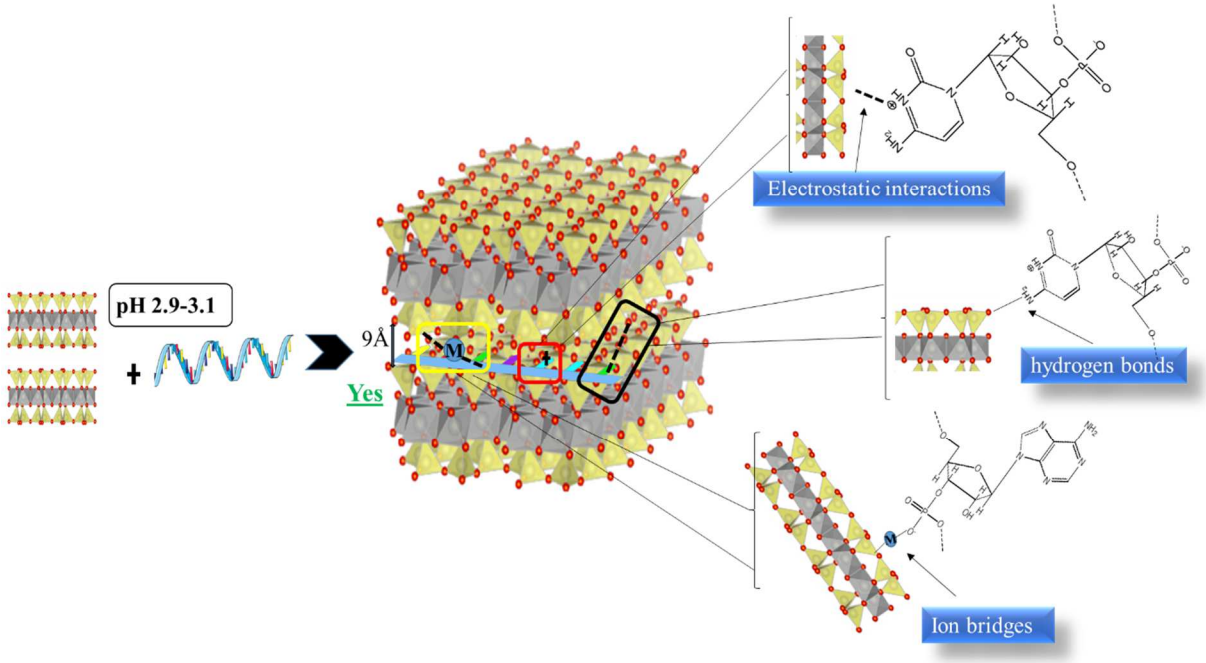
pH 2.9-3.1
9Å
M
Yes
Electrostatic interactions
hydrogen bonds
Ion bridges

393

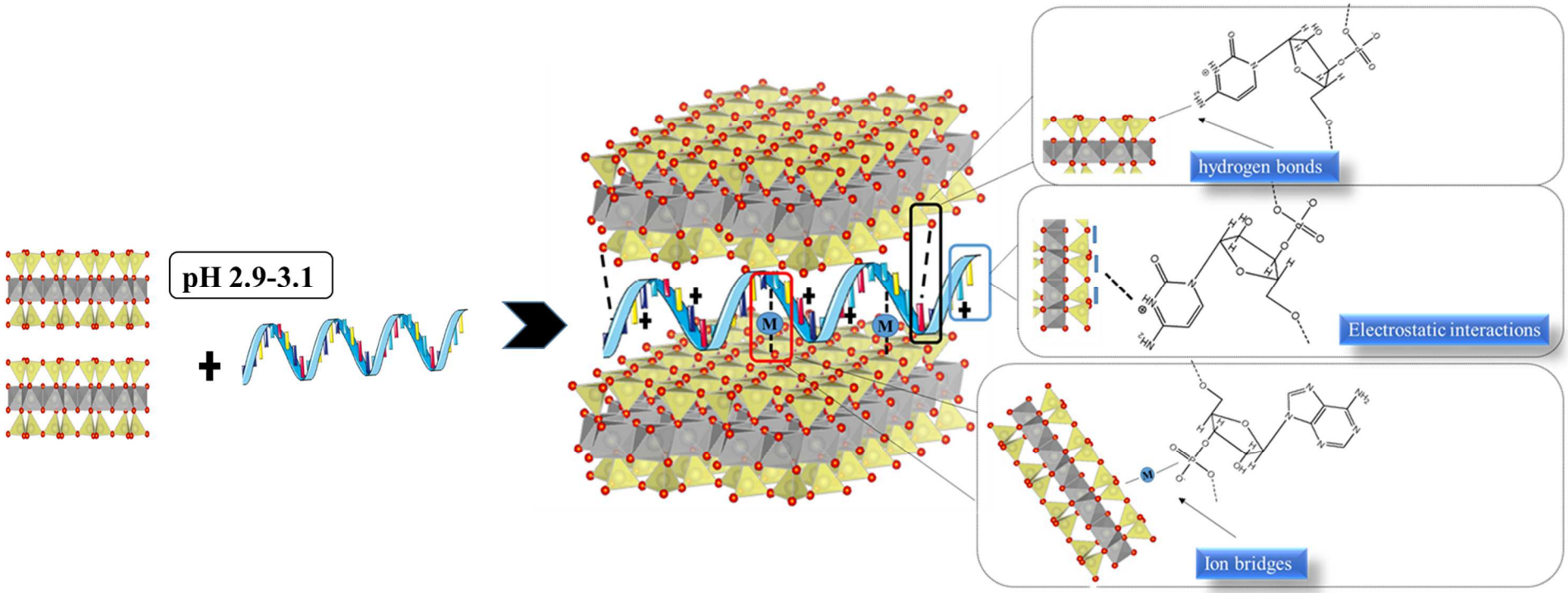


394

395 **Figure 6**. Illustrative scheme for proposed interactions between fragment of RNA and montmorillonite in neutral and acidic medium.

# 5. Conclusions

We have investigated the interaction of an RNA-derived molecule with synthetic montmorillonites having different cations in their interlayer space. The systems were prepared in both neutral and acidic media.

The interaction of the biomolecule with montmorillonites was pH-dependent: the intercalation of RNA in the interlayer space of montmorillonite was largely controlled by electrostatic interactions. At close to neutral pH, the RNA molecules have a significant negative charge and are prevented from entering the interlayer space by electrostatic repulsion from the clay mineral layers. It is likely that RNA is adsorbed on edge sites, maybe with compensating cations acting as ions bridges.

At lower pH values, extensive intercalation occurs, as evidenced by the value of basal spacing observed in XRD. Indeed, the nucleobases are then expected to be partly protonated, resulting in significantly lower negative charges on the RNA molecules. The driving force for intercalation could include contributions of localized electrostatic interactions (between the positively charged aromatic nuclei and the negatively charged clay mineral layers), probably accompanied by H-bonding, and also of coordinative bonding with the interlayer cations. Some authors have suggested that at pH close to 7, van der Waals interactions between the montmorillonite layers and the purine and pyrimidine bases of the nucleotides may also be acting (Kawamura and Ferris, 1999; Ferris, 2006).

Indeed, both FTIR and $^{13}C$ NMR indicate small but significant modifications of the ring carbon atoms local environment. FTIR also shows a rather important shift of the phosphate band. Taken together, these results suggest that both groups are involved in the interaction mechanism. $^{31}P$ NMR shows a surprisingly strong effect of adsorption on the

phosphates, but the direction of the shift does not seem compatible with a coordination to the electropositive compensating cations. Rather, it might be indicative of important configuration changes induced by the intercalation of the RNA backbone into a constrained space.

These results indicate that RNA oligomers and polymers may have interacted effectively with clay minerals, such as montmorillonite, in an acidic medium on the primitive Earth. Such an RNA/montmorillonite interaction may have stabilized and protected RNA molecules from an environment of likely hostile conditions on the primitive earth, such as high UV radiation.

## Acknowledgements

The authors thank CAPES and CNPq (grants 310921-2017-1 and 431727/2016-3) for the financial support.

## References

Akouche, M., Jaber, M., Zins, E.L., Maurel, M.C., Lambert, J.F., Georgelin, T., 2016. Thermal Behavior of d-Ribose Adsorbed on Silica: Effect of Inorganic Salt Coadsorption and Significance for Prebiotic Chemistry. Chem. - A Eur. J. 22, 15834–15846. https://doi.org/10.1002/chem.201601418

Andrushchenko, V., Bouř, P., 2009. Infrared absorption detection of metal ion-deoxyguanosine monophosphate binding: Experimental and theoretical study. J. Phys. Chem. B 113, 283–291. https://doi.org/10.1021/jp8058678

Banyay, M., Sarkar, M., Gräslund, A., 2003. A library of IR bands of nucleic acids in solution. Biophys. Chem. 104, 477–488. https://doi.org/10.1016/S0301-4622(03)00035-8

Benedetti, Edoardo, Bramanti, E., Papineschi, F., Rossi, I., Benedetti, Enzo, 1997.

445 Determination of the relative amount of nucleic acids and proteins in leukemic and
446 normal lymphocytes by means of fourier transform infrared microspectroscopy.
447 Appl. Spectrosc. 51, 792–797. https://doi.org/10.1366/0003702971941304

448 Benetoli, L.O.D.B., De Santana, H., Zaia, C.T.B. V, Zaia, D.A.M., 2008. Adsorption of
449 nucleic acid bases on clays: An investigation using Langmuir and Freundlich
450 isotherms and FT-IR spectroscopy. Monatshefte fur Chemie 139, 753–761.
451 https://doi.org/10.1007/s00706-008-0862-z

452 Bizovská, V., Jankovič, Ľ., Madejová, J., 2018. Montmorillonite modified with
453 unconventional surfactants from the series of octylammonium-based cations:
454 Structural characterization and hydration properties. Appl. Clay Sci. 158, 102–112.
455 https://doi.org/10.1016/j.clay.2018.03.013

456 Black, C.B., Huang, H.W., Cowan, J.A., 1994. Biological coordination chemistry of
457 magnesium, sodium, and potassium ions. Protein and nucleotide binding sites.
458 Coord. Chem. Rev. 135–136, 165–202. https://doi.org/10.1016/0010-
459 8545(94)80068-5

460 Cadars, S., Guégan, R., Garaga, M.N., Bourrat, X., Le Forestier, L., Fayon, F., Huynh,
461 T.V., Allier, T., Nour, Z., Massiot, D., 2012. New insights into the molecular
462 structures, compositions, and cation distributions in synthetic and natural
463 montmorillonite clays. Chem. Mater. 24, 4376–4389.
464 https://doi.org/10.1021/cm302549k

465 Carneiro, C.E.A., Berndt, G., de Souza Junior, I.G., de Souza, C.M.D., Paesano, A., da
466 Costa, A.C.S., di Mauro, E., de Santana, H., Zaia, C.T.B. V., Zaia, D.A.M., 2011.
467 Adsorption of Adenine, Cytosine, Thymine, and Uracil on Sulfide-Modified
468 Montmorillonite: FT-IR, Mössbauer and EPR Spectroscopy and X-Ray
469 Diffractometry Studies. Orig. Life Evol. Biosph. 41, 453–468.
470 https://doi.org/10.1007/s11084-011-9244-3

471 Carrascoza Mayén, J. F.; Rydzewski, J.; Szostak, N.; Blazewicz, J.; Nowak, W.,
472 Prebiotic Soup Components Trapped in Montmorillonite Nanoclay Form New
473 Molecules: Car-Parrinello Ab Initio Simulations. Life 2019, 9,
474 doi: 10.3390/life9020046.

Cases, J.M., Berend, I., Francois, M., Uriot, J.P., Michot, L.J., Thomas, F., 1997. Mechanism of adsorption and desorption of water vapor by homoionic montmorillonite. 3. The $Mg^{2+}$,$Ca^{2+}$,$Sr^{2+}$ and $Ba^{2+}$ exchanged forms. Clays Clay Miner. 45, 8–22.

Cavalcante, M.S., Paz, S.P.A., Angélica, R.S., Ito, E.N., Freitas Neves, R., 2016. Organophilization of a Brazilian Mg-montmorillonite without prior sodium activation. Clay Miner. 51, 39–54. https://doi.org/10.1180/claymin.2016.051.1.04

Cavalcanti, G.R.S., Rodrigues, F., Zhuang, G., Balme, S., Janot, J.M., Fonseca, M.G., Jaber, M., 2021. Inorganic-organic hybrid pigments based on carminic acid and clay minerals. Dye. Pigment. 190. https://doi.org/10.1016/j.dyepig.2021.109306

Chang, C. jer, Diaz, L.E., Woolfenden, W.R., Grant, D.M., 1982. Solid-State Carbon-13 Nuclear Magnetic Resonance Study of Ribonucleosides and Ribonucleic Acid. J. Org. Chem. 47, 5318–5321. https://doi.org/10.1021/jo00148a018

Chang, P.H., Jiang, W.T., Li, Z., 2018. Mechanism of tyramine adsorption on Ca-montmorillonite. Sci. Total Environ. 642, 198–207. https://doi.org/10.1016/j.scitotenv.2018.05.190

Costa, T.M.H., Gallas, M.R., Benvenutti, E. V., Da Jornada, J.A.H., 1997. Infrared and thermogravimetric study of high pressure consolidation in alkoxide silica gel powders. J. Non. Cryst. Solids 220, 195–201. https://doi.org/10.1016/S0022-3093(97)00236-6

da Silva, J.C.S., França, D.B., Rodrigues, F., Oliveira, D.M., Trigueiro, P., Silva Filho, E.C., Fonseca, M.G., 2021. What happens when chitosan meets bentonite under microwave-assisted conditions? Clay-based hybrid nanocomposites for dye adsorption. Colloids Surfaces A Physicochem. Eng. Asp. 609, 125584. https://doi.org/10.1016/j.colsurfa.2020.125584

Duguid, J., Bloomfield, V.A., Benevides, J., Thomas, G.J., 1993. Raman spectroscopy of DNA-metal complexes. I. Interactions and conformational effects of the divalent cations: Mg, Ca, Sr, Ba, Mn, Co, Ni, Cu, Pd, and Cd. Biophys. J. 65, 1916–1928. https://doi.org/10.1016/S0006-3495(93)81263-3

Eder, A.H., Rode, B.M., 1994. Influence of alkali- and alkaline-earth-metal cations on the “salt-induced peptide formation” reaction. J. Chem. Soc. Dalt. Trans. 1125–1130. https://doi.org/10.1039/DT9940001125

Escamilla-Roa, E., Huertas, F.J., Hernández-Laguna, A., Sainz-Díaz, C.I., 2017. A DFT study of the adsorption of glycine in the interlayer space of montmorillonite. Phys. Chem. Chem. Phys. 19, 14961–14971. https://doi.org/10.1039/c7cp02300f

Ferris, J.P., 2006. Montmorillonite-catalysed formation of RNA oligomers: The possible role of catalysis in the origins of life. Philos. Trans. R. Soc. B Biol. Sci. 361, 1777–1786. https://doi.org/10.1098/rstb.2006.1903

Feuillie, C., Daniel, I., Michot, L.J., Pedreira-Segade, U., 2013. Adsorption of nucleotides onto Fe-Mg-Al rich swelling clays. Geochim. Cosmochim. Acta 120, 97–108. https://doi.org/10.1016/j.gca.2013.06.021

Feuillie, C., Sverjensky, D.A., Hazen, R.M., 2015. Attachment of ribonucleotides on α-alumina as a function of ph, ionic strength, and surface loading. Langmuir 31, 240–248. https://doi.org/10.1021/la504034k

Fornaro, T., Brucato, J.R., Feuillie, C., Sverjensky, D.A., Hazen, R.M., Brunetto, R., D’Amore, M., Barone, V., 2018. Binding of Nucleic Acid Components to the Serpentinite-Hosted Hydrothermal Mineral Brucite. Astrobiology 18, 989–1007. https://doi.org/10.1089/ast.2017.1784

França, D.B., Trigueiro, P., Silva Filho, E.C., Fonseca, M.G., Jaber, M., 2020. Monitoring diclofenac adsorption by organophilic alkylpyridinium bentonites. Chemosphere 242, 125109. https://doi.org/10.1016/j.chemosphere.2019.125109

Franchi, M., Ferris, J.P., Gallori, E., 2003. Cations as mediators of the adsorption of nucleic acids on clay surfaces in prebiotic environments. Orig. Life Evol. Biosph. 33, 1–16. https://doi.org/10.1023/A:1023982008714

Fujiwara, T., Sugase, K., Akutsu, H., Kainosho, M., Ono, A., Ono, A.M., 1995. 13C—13C and 13C—15N Dipolar Correlation NMR of Uniformly Labeled Organic Solids for the Complete Assignment of Their 13C and 15N Signals: An Application to Adenosine. J. Am. Chem. Soc. 117, 11351–11352.

https://doi.org/10.1021/ja00150a038

Garg, N., Skibsted, J., 2014. Thermal activation of a pure montmorillonite clay and its reactivity in cementitious systems. J. Phys. Chem. C 118, 11464–11477. https://doi.org/10.1021/jp502529d

Gopinath, S., Sugunan, S., 2007. Enzymes immobilized on montmorillonite K 10: Effect of adsorption and grafting on the surface properties and the enzyme activity. Appl. Clay Sci. 35, 67–75. https://doi.org/10.1016/j.clay.2006.04.007

Greaves, M.P., Wilson, M.J., 1969. The adsorption of nucleic acids by montmorillonite. Soil Biol. Biochem. 1, 317–323. https://doi.org/10.1016/0038-0717(69)90014-5

Guillermin, D., Debroise, T., Trigueiro, P., de Viguerie, L., Rigaud, B., Morlet-Savary, F., Balme, S., Janot, J.M., Tielens, F., Michot, L., Lalevee, J., Walter, P., Jaber, M., 2019. New pigments based on carminic acid and smectites: A molecular investigation. Dye. Pigment. 160, 971–982. https://doi.org/10.1016/j.dyepig.2018.07.021

Gujjari, A., Rodriguez, B. V., Pescador, J., Maeder, C., Beall, G.W., Lewis, L.K., 2018. Factors affecting the association of single- and double-stranded RNAs with montmorillonite nanoclays. Int. J. Biol. Macromol. 109, 551–559. https://doi.org/10.1016/j.ijbiomac.2017.12.124

Hao, J., Mokhtari, M., Pedreira-Segade, U., Michot, L.J., Daniel, I., 2019. Transition Metals Enhance the Adsorption of Nucleotides onto Clays: Implications for the Origin of Life. ACS Earth Sp. Chem. 3, 109–119. https://doi.org/10.1021/acsearthspacechem.8b00145

Hashizume, H., van der Gaast, S., Theng, B.K.G., 2010. Adsorption of adenine, cytosine, uracil, ribose, and phosphate by Mg-exchanged montmorillonite. Clay Miner. 45, 469–475. https://doi.org/10.1180/claymin.2010.045.4.469

Izawa, M.R.M., Nesbitt, H.W., MacRae, N.D., Hoffman, E.L., 2010. Composition and evolution of the early oceans: Evidence from the Tagish Lake meteorite. Earth Planet. Sci. Lett. 298, 443–449. https://doi.org/10.1016/j.epsl.2010.08.026

561 Jaber, M., Georgelin, T., Bazzi, H., Costa-Torro, F., Lambert, J.-F., Bolbach, G.,
562 Clodic, G., 2014. Selectivities in Adsorption and Peptidic Condensation in the
563 (Arginine and Glutamic Acid)/Montmorillonite Clay System. J. Phys. Chem. C
564 118, 25447–25455. https://doi.org/10.1021/jp507335e

565 Jaber, M., Miehé-Brendlé, J., 2008. Synthesis, characterization and applications of 2:1
566 phyllosilicates and organophyllosilicates: Contribution of fluoride to study the
567 octahedral sheet. Microporous Mesoporous Mater. 107, 121–127.
568 https://doi.org/10.1016/j.micromeso.2007.02.047

569 Jaber, M., Miéhé-Brendlé, J., 2005. Influence du milieu de synthése sur la cristallisation
570 de saponite: Proposition de mécanisme réactionnel en milieux acide et basique.
571 Comptes Rendus Chim. 8, 229–234. https://doi.org/10.1016/j.crci.2004.10.025

572 James Cleaves, H., Michalkova Scott, A., Hill, F.C., Leszczynski, J., Sahai, N., Hazen,
573 R., 2012. Mineral-organic interfacial processes: Potential roles in the origins of
574 life. Chem. Soc. Rev. 41, 5502–5525. https://doi.org/10.1039/c2cs35112a

575 Jelavić, S., Tobler, D.J., Hassenkam, T., De Yoreo, J.J., Stipp, S.L.S., Sand, K.K., 2017.
576 Prebiotic RNA polymerisation: energetics of nucleotide adsorption and
577 polymerisation on clay mineral surfaces. Chem. Commun. 53, 12700–12703.
578 https://doi.org/10.1039/C7CC04276K

579 Kawamura, K., Ferris, J.P., 1999. Clay catalysis of oligonucleotide formation: Kinetics
580 of the reaction of the 5'-phosphorimidazolides of nucleotides with the non-basic
581 heterocycles uracil and hypoxanthine. Orig. Life Evol. Biosph. 29, 563–591.
582 https://doi.org/10.1023/A:1006648524187

583 Kim, S.H., Sussman, J.L., Suddath, F.L., Quigley, G.J., McPherson, A., Wang, A.H.,
584 Seeman, N.C., RICH, A., 1974. The general structure of transfer RNA molecules.
585 Proc. Natl. Acad. Sci. U. S. A. 71, 4970–4974.
586 https://doi.org/10.1073/pnas.71.12.4970

587 Kumar, A., Singh, B., 2013. Zn2+-induced folding of RNA to produce honeycomb-like
588 RNA-mediated fluorescing Zn2+/PbSe nanostructures. J. Phys. Chem. C 117,
589 5386–5396. https://doi.org/10.1021/jp309822w

590 Lapper, R.D., Mantsch, H.H., Smith, I.C.P., 1973. A Carbon-13 Nuclear Magnetic
591 Resonance Study of the Conformations of 3′,5′-Cyclic Nucleotides. J. Am. Chem.
592 Soc. 95, 2878–2880. https://doi.org/10.1021/ja00790a024

593 Lawless, J. G.; Banin, A.; Church, F. M.; Mazzurco, J.; Huff, R.; Kao, J.; Cook, A.;
594 Lowe, T.; Orenberg, J. B.; Eselson, E., pH Profile of the Adsorption of Nucleotides
595 onto Montmorillonite.1. Selected Homoionic Clays. *Orig. Life Evol. Biosph.* **1985,**
596 *15* (2), 77-88.

597

598 Legault, P., Pardi, A., 1994. 31P Chemical Shift as a Probe of Structural Motifs in
599 RNA. J. Magn. Reson. Ser. B. https://doi.org/10.1006/jmrb.1994.1012

600 Leonarski, F., D'Ascenzo, L., Auffinger, P., 2017. Mg2+ ions: Do they bind to
601 nucleobase nitrogens? Nucleic Acids Res. 45, 987–1004.
602 https://doi.org/10.1093/nar/gkw1175

603 Lepoitevin, M., Jaber, M., Guégan, R., Janot, J.M., Dejardin, P., Henn, F., Balme, S.,
604 2014. BSA and lysozyme adsorption on homoionic montmorillonite: Influence of
605 the interlayer cation. Appl. Clay Sci. 95, 396–402.
606 https://doi.org/10.1016/j.clay.2014.05.003

607 Liu, J., Zhao, Y., Li, H., Chen, T., Song, S., 2017. Stability of Na-montmorillonite
608 suspension in the presence of different cations and valences. J. Dispers. Sci.
609 Technol. 38, 1035–1040. https://doi.org/10.1080/01932691.2016.1218344

610 Madejová, J., Gates, W.P., Petit, S., 2017. IR Spectra of Clay Minerals, Developments
611 in Clay Science. Elsevier. https://doi.org/10.1016/B978-0-08-100355-8.00005-9

612 Maderia, M., Horton, T.E., DeRose, V.J., 2000. Metal Interactions with a GAAA RNA
613 Tetraloop Characterized by 31 P NMR and Phosphorothioate Substitutions †.
614 Biochemistry 39, 8193–8200. https://doi.org/10.1021/bi000140l

615 Manzano, I., Zydney, A.L., 2017. Quantitative study of RNA transmission through
616 ultrafiltration membranes. J. Memb. Sci. 544, 272–277.
617 https://doi.org/10.1016/j.memsci.2017.09.042

618 Marsh, A., Heath, A., Patureau, P., Evernden, M., Walker, P., 2018. Alkali activation
619 behaviour of un-calcined montmorillonite and illite clay minerals. Appl. Clay Sci.
620 166, 250–261. https://doi.org/10.1016/j.clay.2018.09.011

621 Martin, R.B., 1985. Nucleoside Sites for Transition Metal Ion Binding. Acc. Chem. Res.
622 18, 32–38. https://doi.org/10.1021/ar00110a001

623 Mignon, P., Sodupe, M., 2012. Theoretical study of the adsorption of DNA bases on the
624 acidic external surface of montmorillonite. Phys. Chem. Chem. Phys. 14, 945–954.
625 https://doi.org/10.1039/c1cp22454a

626 Mignon, P., Ugliengo, P., Sodupe, M., 2009. Theoretical study of the adsorption of
627 RNA/DNA bases on the external surfaces of Na+-montmorillonite. J. Phys. Chem.
628 C 113, 13741–13749. https://doi.org/10.1021/jp901699q

629 Moore, D.M., Reynolds, R.C., 1997. X-Ray Diffraction and the Identification and
630 Analysis of Clay Minerals. Oxford University Press, New York.

631 Pedreira-Segade, U., Feuillie, C., Pelletier, M., Michot, L.J., Daniel, I., 2016.
632 Adsorption of nucleotides onto ferromagnesian phyllosilicates: Significance for the
633 origin of life. Geochim. Cosmochim. Acta 176, 81–95.
634 https://doi.org/10.1016/j.gca.2015.12.025

635 Pedreira-Segade, U., Michot, L.J., Daniel, I., 2018. Effects of salinity on the adsorption
636 of nucleotides onto phyllosilicates. Phys. Chem. Chem. Phys. 20, 1938–1952.
637 https://doi.org/10.1039/c7cp07004g

638 Pentrák, M., Bizovská, V., Madejová, J., 2012. Near-IR study of water adsorption on
639 acid-treated montmorillonite. Vib. Spectrosc. 63, 360–366.
640 https://doi.org/10.1016/j.vibspec.2012.07.012

641 Pentrák, M., Hronský, V., Pálková, H., Uhlík, P., Komadel, P., Madejová, J., 2018.
642 Alteration of fine fraction of bentonite from Kopernica (Slovakia) under acid
643 treatment: A combined XRD, FTIR, MAS NMR and AES study. Appl. Clay Sci.
644 163, 204–213. https://doi.org/10.1016/j.clay.2018.07.028

645 Pyle, A.M., 2002. Metal ions in the structure and function of RNA. J. Biol. Inorg.

Chem. 7, 679–690. https://doi.org/10.1007/s00775-002-0387-6

Reinholdt, M., Miehé-Brendlé, J., Delmotte, L., Le Dred, R., Tuilier, M.-H., 2005. Synthesis and characterization of montmorillonite-type phyllosilicates in a fluoride medium. Clay Miner. 40, 177–190. https://doi.org/10.1180/0009855054020164

Reinholdt, M., Miehé-Brendlé, J., Delmotte, L., Tuilier, M.-H., le Dred, R., Cortès, R., Flank, A.-M., 2001. Fluorine Route Synthesis of Montmorillonites Containing Mg or Zn and Characterization by XRD, Thermal Analysis, MAS NMR, and EXAFS Spectroscopy. Eur. J. Inorg. Chem. 2001, 2831–2841. https://doi.org/10.1002/1099-0682(200111)2001:11<2831::AID-EJIC2831>3.0.CO;2-6

Rodrigues, F., Georgelin, T., Gabant, G., Rigaud, B., Gaslain, F., Zhuang, G., Gardênnia da Fonseca, M., Valtchev, V., Touboul, D., Jaber, M., 2019. Confinement and Time Immemorial: Prebiotic Synthesis of Nucleotides on a Porous Mineral Nanoreactor. J. Phys. Chem. Lett. 10, 4192–4196. https://doi.org/10.1021/acs.jpclett.9b01448

Ruiz-Mirazo, K., Briones, C., De La Escosura, A., 2014. Prebiotic systems chemistry: New perspectives for the origins of life. Chem. Rev. 114, 285–366. https://doi.org/10.1021/cr2004844

Saka, E.E., Güler, C., 2006. The effects of electrolyte concentration, ion species and pH on the zeta potential and electrokinetic charge density of montmorillonite. Clay Miner. 41, 853–861. https://doi.org/10.1180/0009855064140224

Sanjay, G., Sugunan, S., 2006. Enhanced pH and thermal stabilities of invertase immobilized on montmorillonite K-10. Food Chem. 94, 573–579. https://doi.org/10.1016/j.foodchem.2004.12.043

Şans, B.E., Güven, O., Esenli, F., Çelik, M.S., 2017. Contribution of cations and layer charges in the smectite structure on zeta potential of Ca-bentonites. Appl. Clay Sci. 143, 415–421. https://doi.org/10.1016/j.clay.2017.04.016

Santos, S.S.G., Silva, H.R.M., de Souza, A.G., Alves, A.P.M., da Silva Filho, E.C., Fonseca, M.G., 2015. Acid-leached mixed vermiculites obtained by treatment with

675 nitric acid. Appl. Clay Sci. 104, 286–294.
676 https://doi.org/10.1016/j.clay.2014.12.008

677 Schnetzer, F., Johnston, C.T., Premachandra, G.S., Giraudo, N., Schuhmann, R.,
678 Thissen, P., Emmerich, K., 2017. Impact of Intrinsic Structural Properties on the
679 Hydration of 2:1 Layer Silicates. ACS Earth Sp. Chem. 1, 608–620.
680 https://doi.org/10.1021/acsearthspacechem.7b00091

681 Shamsuddin, R.M., Verbeek, C.J.R., Lay, M.C., 2014. Producing protein intercalated
682 bentonite - Equilibrium, kinetics and physical properties of gelatin-bentonite
683 system. Appl. Clay Sci. 87, 52–60. https://doi.org/10.1016/j.clay.2013.11.023

684 Sheng, X., Qin, C., Yang, B., Hu, X., Liu, C., Waigi, M.G., Li, X., Ling, W., 2019.
685 Metal cation saturation on montmorillonites facilitates the adsorption of DNA via
686 cation bridging. Chemosphere 235, 670–678.
687 https://doi.org/10.1016/j.chemosphere.2019.06.159

688 Theng, B. K. G., 1982, 'Clay-polymer interactions: Summary and perspectives', Clays
689 Clay Miner. 30, 1−10.

690 Tripathi, M.; Khilari, R.; Thakur, Y.; Verma, B.; Pardhi, M.; Pande, R.,
691 Oxovanadium complex as potential nucleic acid binder. J. Macromol. Sci. A: Pure
692 Appl. Chem. 2017, 54, 85-90.

693 Trigueiro, P., Pedetti, S., Rigaud, B., Balme, S., Janot, J.-M., dos Santos, I.M.G.,
694 Gougeon, R., Fonseca, M.G., Georgelin, T., Jaber, M., 2018a. Going through the
695 wine fining: Intimate dialogue between organics and clays. Colloids Surfaces B
696 Biointerfaces 166, 79–88. https://doi.org/10.1016/j.colsurfb.2018.02.060

697 Trigueiro, P., Pereira, F.A.R., Guillermin, D., Rigaud, B., Balme, S., Janot, J.-M., dos
698 Santos, I.M.G., Fonseca, M.G., Walter, P., Jaber, M., 2018b. When anthraquinone
699 dyes meet pillared montmorillonite: Stability or fading upon exposure to light?
700 Dye. Pigment. 159, 384–394. https://doi.org/10.1016/j.dyepig.2018.06.046

701 Tsuboi, M., 1970. Application of Infrared Spectroscopy to Structure Studies of Nucleic
702 Acids. Appl. Spectrosc. Rev. 3, 45–90.
703 https://doi.org/10.1080/05704927008081687

704 Viennet, J.C., Bernard, S., Le Guillou, C., Jacquemot, P., Delbes, L., Balan, E., Jaber,
705 M., 2020. Influence of the nature of the gas phase on the degradation of RNA
706 during fossilization processes. Appl. Clay Sci. 191, 105616.
707 https://doi.org/10.1016/j.clay.2020.105616

708 Villafañe-Barajas, S. A.; Baú, J. P. T.; Colín-García, M.; Negrón-Mendoza, A.;
709 Heredia-Barbero, A.; Pi-Puig, T.; Zaia, D. A. M., Salinity Effects on the
710 Adsorption of Nucleic Acid Compounds on Na-Montmorillonite: a Prebiotic
711 Chemistry Experiment. Orig. Life Evol. Biosph. 2018, 48 (2), 181-200. DOI:
712 10.1007/s11084-018-9554-9.

713

714 Wu, L., Liao, L., Lv, G., 2015. Influence of interlayer cations on organic intercalation of
715 montmorillonite. J. Colloid Interface Sci. 454, 1–7.
716 https://doi.org/10.1016/j.jcis.2015.04.021

717 Xie, H., Wan, Z., Liu, S., Zhang, Y., Tan, J., Yang, H., 2019. Charge-Dependent
718 Regulation in DNA Adsorption on 2D Clay Minerals. Sci. Rep. 9, 1–10.
719 https://doi.org/10.1038/s41598-019-41093-5

720 Yu, W.H., Li, N., Tong, D.S., Zhou, C.H., Lin, C.X., Xu, C.Y., 2013. Adsorption of
721 proteins and nucleic acids on clay minerals and their interactions: A review. Appl.
722 Clay Sci. 80–81, 443–452. https://doi.org/10.1016/j.clay.2013.06.003

723 Yukselen, Y., Erzin, Y., 2008. Artificial neural networks approach for zeta potential of
724 Montmorillonite in the presence of different cations. Environ. Geol. 54, 1059–
725 1066. https://doi.org/10.1007/s00254-007-0872-x

726

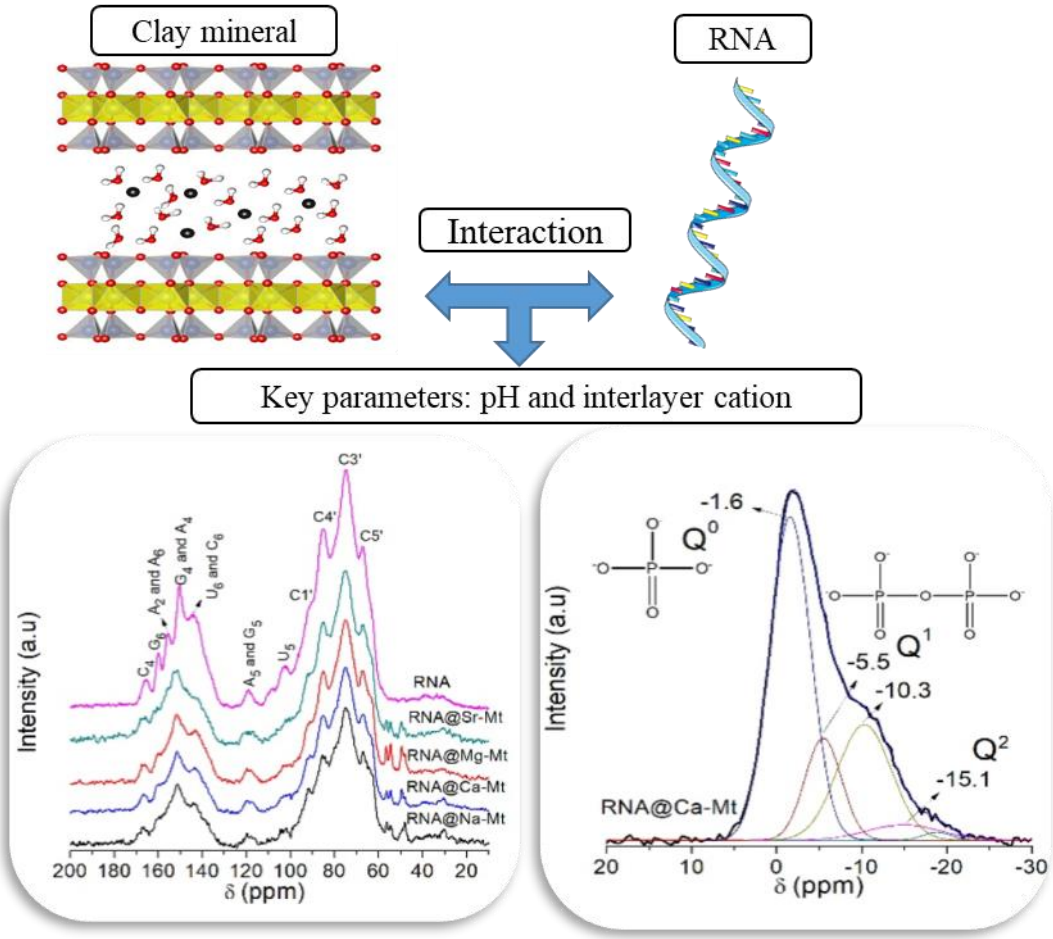


Full-size image:

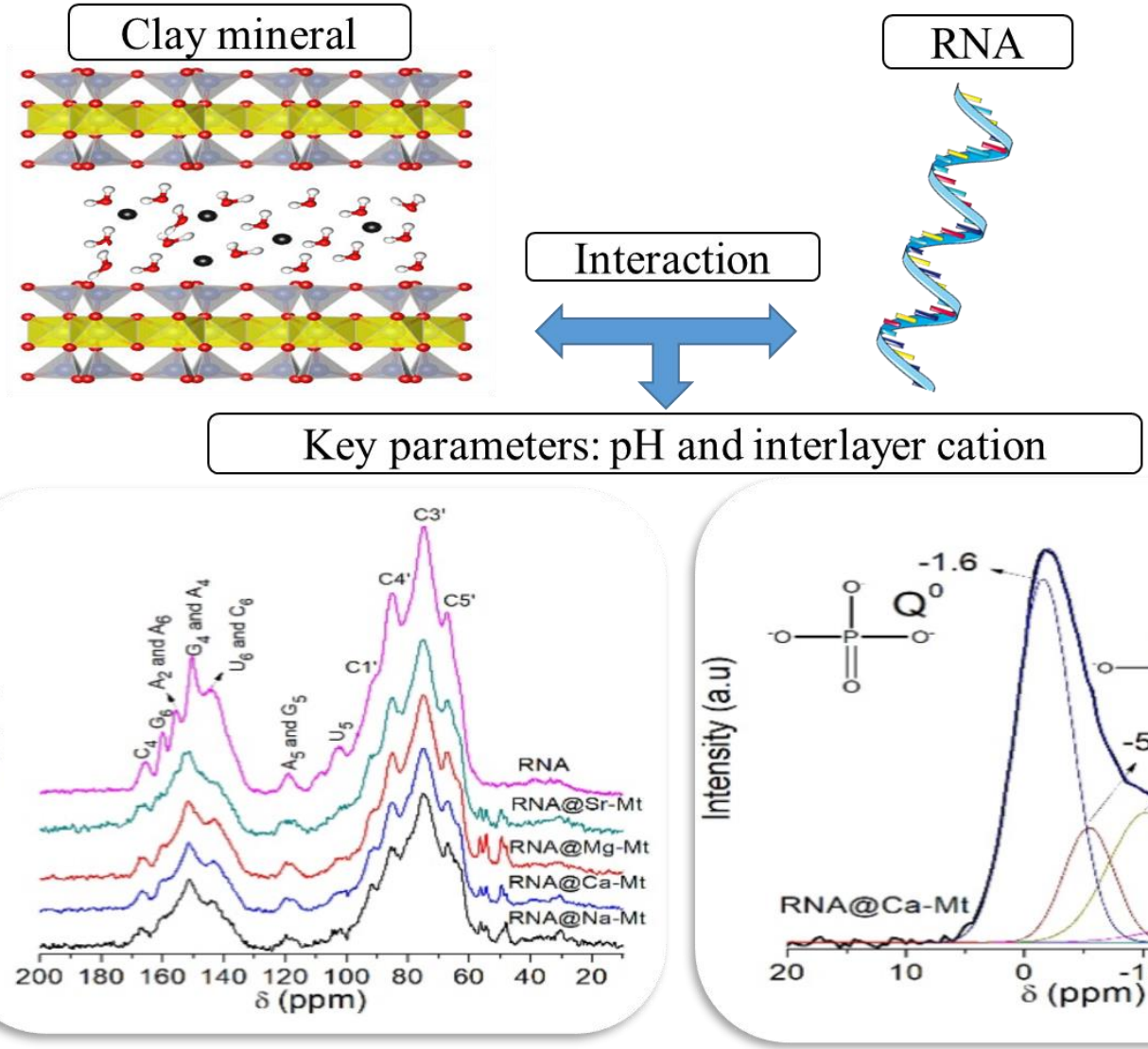
Clay mineral
RNA
Interaction
Key parameters: pH and interlayer cation
Intensity (a.u)
δ (ppm)
C3'
C4'
C5'
C1'
C4 G8 A2 and A6
G4 and A4
U6 and C6
A5 and G5
U5
RNA
RNA@Sr-Mt
RNA@Mg-Mt
RNA@Ca-Mt
RNA@Na-Mt
200 180 160 140 120 100 80 60 40 20
-1.6
Q0
Q1
Q2
-5.5
-10.3
-15.1
RNA@Ca-Mt
20 10 0 -10 -20 -30